Tailor-Made Polyamide Membranes for Water Desalination

Wansuk Choi,[†,#] Joung-Eun Gu,[‡,§,#] Sang-Hee Park,[†,⊥] Seyong Kim,[†] Joona Bang,[†] Kyung-Youl Baek,[⊥] Byoungnam Park,[∥] Jong Suk Lee,[*,‡] Edwin P. Chan,[*,+] and Jung-Hyun Lee[*,†]

[†]Department of Chemical and Biological Engineering, Korea University, 5-1 Anam-dong, Seongbuk-gu, Seoul 136-713, Republic of Korea, [‡]Center for Environment, Health and Welfare Research and [⊥]Center for Materials Architecturing, Korea Institute of Science and Technology (KIST), 39-1 Hawolgok-dong, Seongbuk-gu, Seoul 136-791, Republic of Korea, [§]School of Urban and Environmental Engineering, Ulsan National Institute of Science and Technology, UNIST-gil 50, Ulsan 689-798, Republic of Korea, [∥]Department of Materials Science and Engineering, Hongik University, 72-1 Sangsu-dong, Mapo-gu, Seoul 121-791, Republic of Korea, and [+]Materials Science and Engineering Division, The National Institute of Standards and Technology (NIST), 100 Bureau Drive, Gaithersburg, Maryland 20899, United States. [#]These authors contributed equally.

ABSTRACT Independent control of the extrinsic and intrinsic properties of the polyamide (PA) selective layer is essential for designing thin-film composite (TFC) membranes with performance characteristics required for water purification applications besides seawater desalination. Current commercial TFC membranes fabricated *via* the well-established interfacial polymerization (IP) approach yield materials that are far from ideal because their layer thickness, surface roughness, polymer chemistry, and network structure cannot be separately tailored. In this work, tailor-made PA-based desalination membranes based on molecular layer-by-layer (mLbL) assembly are presented. The mLbL technique enables the construction of an ultrathin and highly cross-linked PA seletive layer in a precisely and independently controlled manner. The mLbL-assembled TFC membranes exhibit significant enhancements in performance compared to their IP-assembled counterparts. A maximum sodium chloride rejection of 98.2% is achieved along with over 2.5 times higher water flux than the IP-assembled counterpart. More importantly, this work demonstrates the broad applicability of mLbL in fabricating a variety of PA-based TFC membranes with nanoscale control of the selective layer thickness and roughness independent of the specific polyamide chemistry.

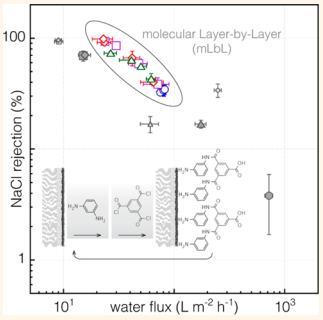

KEYWORDS: molecular layer-by-layer · polyamide · thin film composite membrane · reverse osmosis · water desalination

Reverse osmosis (RO) is currently the most widely used technology for seawater desalination and water treatment because it is the most energy-efficient means for removing salt from seawater.[1,2] As the name implies, RO is a high pressure-driven separation process where a pressure exceeding the osmotic pressure between the salt ions and pure water is applied to selectively permeate water across a semipermeable membrane while retaining the salt ions. The key component of the RO process is the asymmetric thin-film composite (TFC) membrane comprising of a highly cross-linked polyamide (PA) selective layer on a hierarchical porous polymeric support structure.[3] Separation or screening of the salt ions and pure water occurs within this PA selective layer. Therefore, both the extrinsic (thickness, roughness, surface functionality) and intrinsic (chemistry, molecular topology, molecular homogeneity) properties of this PA layer are critical to controlling the water flux, salt flux, and selectivity between the salt ions and water.

The PA selective layers of current state-of-the-art TFC membranes are made by variations of the interfacial polymerization (IP) technique that was pioneered by Cadotte in the late 1970s.[4] The typical IP process involves impregnating a porous polymeric support with an aqueous diamine solution and subsequent exposure to an organic triacid chloride solution. Polymerization reaction occurs at the organic phase of the water−oil interface formed by two immiscible solutions due to the negligible solubility of acid chlorides in water and moderate solubility of amines in organic solvents. Amine monomers diffuse from the aqueous phase to the organic phase to rapidly react with the acid chloride, and the IP reaction proceeds *via* a diffusion-limited process.[5−8] Depending on the process variables such as reactivity, solubility, and

* Address correspondence to jong.lee@kist.re.kr, edwin.chan@nist.gov, leejhyyy@korea.ac.kr.

Received for review September 19, 2014 and accepted December 30, 2014.

Published online December 30, 2014
10.1021/nn505318v

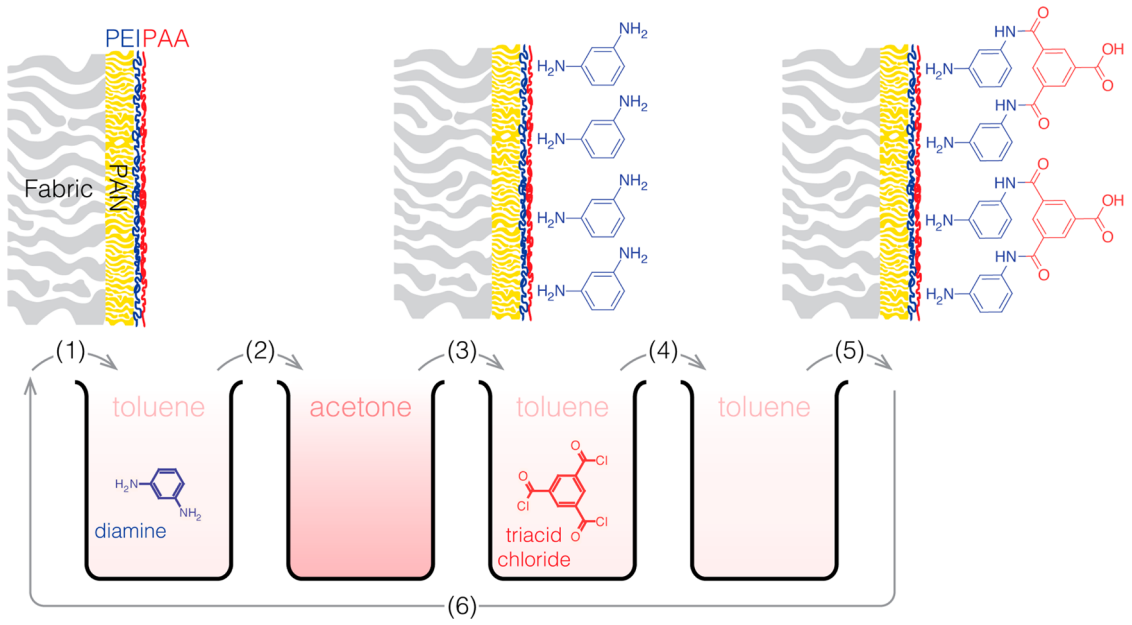

Figure 1. Molecular layer-by-layer (mLbL) approach for fabricating polyamide (PA) thin film composite (TFC) membranes. (1) Dipping the PEI/PAA polyelectrolyte bilayer-coated PAN membrane into a diamine solution in toluene. (2) Rinsing the membrane with acetone to remove the unreacted diamine monomers. (3) Dipping the membrane into a triacid chloride solution in toluene. (4) Rinsing with toluene to remove the unreacted triacid chloride. (5) Finishing one mLbL deposition cycle. (6) Repeating the deposition steps 1−4 until the desired number of deposition cycles is obtained.

diffusivity of the specific monomers, surface tension, and viscosity of solvents, *etc*., the IP process produces an ultrathin PA layer with a unique surface morphology and a film thickness ranging from ~20 nm to ~200 nm. IP satisfies many of the requirements for a commercial TFC because it facilitates scalable manufacturing of a dense and ultrathin PA semipermeable membrane. However, the IP-assembled TFCs are far from ideal as both the extrinsic and intrinsic properties of the PA layer are largely dictated by the process variables mentioned above.[9−12] In addition to film thickness, properties including surface roughness, homogeneity of the PA network structure, and chemical functionality are highly dependent on the process variables. Since the process variables are convoluted with one another in IP, it is not straightforward to control one property without affecting another property,[10] which leads to difficulty in fabricating TFC membranes with well-defined and deconvoluted intrinsic and extrinsic properties.

In an effort to overcome some of the limitations of IP for fabricating TFC membranes, we have recently devised an alternative approach termed molecular layer-by-layer (mLbL).[13,14] The mLbL approach is analogous to atomic layer deposition and polymer layer-by-layer (LbL), where the PA layer is constructed one monomer layer at a time *via* alternate cross-linking of the diamine and triacid chloride. We demonstrated that mLbL can successfully fabricate PA TFC membranes that exceed the RO performance of the IP-assembled membranes.[14] The performance enhancements of these mLbL-assembled TFC membranes are associated with precise control over the PA layer thickness, network structure, and surface roughness facilitated by mLbL.

This seminal work was limited to studying the mLbL-assembled TFC membranes fabricated using *m*-phenylenediamine (MPD) and trimesoyl chloride (TMC) as the diamine and triacid chloride monomers, respectively. Because the work did not apply mLbL to the fabrication of TFC membranes using other PA monomer chemistries, it did not address the primary limitation of IP, which is the inability to decouple the extrinsic and intrinsic properties of the PA layer. Independent control over the extrinsic and intrinsic properties of the PA is vitally important in designing membranes with performance characteristics required for water purification applications besides just seawater desalination. In this contribution, we address these questions by applying mLbL to fabricate TFC membranes using other PA monomer chemistries. We measure the water and salt permeation of these mLbL-assembled membranes and compare them with their IP counterparts to show that the performance of the mLbL-assembled membranes is not only superior but can be tailored because the selective layer thickness, roughness, and polyamide chemistry can be independently controlled.

RESULTS AND DISCUSSION

We apply both mLbL (see the Methods and Figure 1) and IP (see the Methods) approaches to fabricate TFC membranes with four different aromatic PA chemistries (one semiaromatic and three fully aromatic PAs

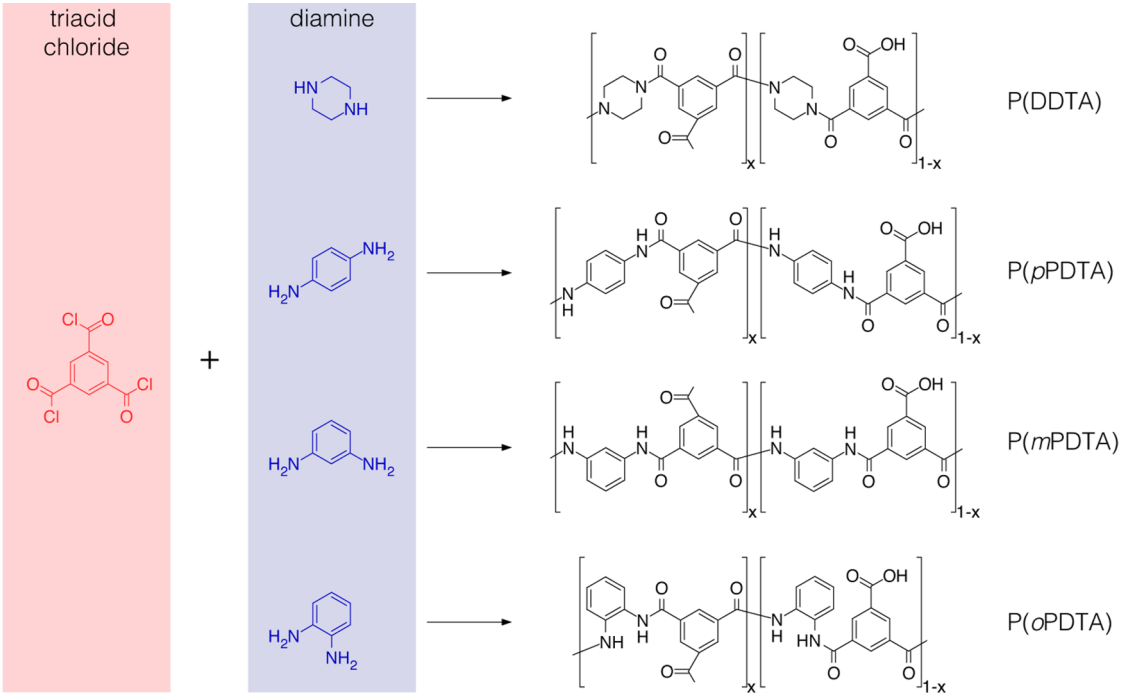

Figure 2. Four PAs investigated in this work: poly(diethylenediamine trisamide) (P(DDTA)), poly(*p*-phenylenediamine trisamide) (P(*p*PDTA)), poly(*m*-phenylenediamine trisamide) (P(*m*PDTA)), and poly(*o*-phenylenediamine trisamide) (P(*o*PDTA)).

with different isomeric positions of amine moieties). The chemical structures of the four PAs were designed by varying the type of diamines while using the same triacid chloride (trimesoyl chloride, TMC) as shown in Figure 2. We were interested in investigating the effect of aromaticity and isomerism of these PAs on the membrane performance because they are commonly used as the selective layers of TFC membranes for RO or nanofiltration (NF) applications.

To fabricate a mLbL-assembled PA TFC membrane, we begin by hydrolyzing a commercial poly(acrylonitrile) (PAN) ultrafiltration porous support with NaOH (HPAN) and then coating it with a single bilayer of polyelectrolyte layer-by-layer (LbL) assembly as an interlayer. The hydrolysis treament enhances the negative charge density and hydrophilicity of the PAN surface.[11] The two polyions used are branched poly(ethylenimine) (PEI) and poly(acrylic acid) (PAA). Branched PEI was selected because (1) it is positively charged, thus facilitaing adsorption onto the negatively charged PAN surface, and (2) its large molecular size can effectively block the pores of the PAN, thus allowing the fabrication of a uniform and defect-free PA selective layer *via* subsequent mLbL.[14] PAA was selected since it contains a high density of negatively charged carboxylic acid groups that facilitate electrostatic interaction and/or hydrogen bonding with the positively charged diamine monomer in the first mLbL deposition. Next, the polyelectrolyte LbL-coated PAN support was alternatively dipped into the two monomer solutions and rinsed with the appropriate rinse solvents after each dipping step to yield the cross-linked PA selective layer. For the poly(*m*-phenylenediamine trisamide) (P(*m*PDTA)) system, the diamine and triacid chloride monomers are *m*-phenylenediamine (MPD) and TMC, respectively. This mLbL deposition procedure was repeated until the desired cycle number was obtained with one cycle represented by the reaction between the diamine and triacid chloride as illustrated in Figure 1. Each PA system was fabricated by mLbL with the cycle numbers of 0, 1, 5, 10, and 15. We also fabricated IP-assembled PA TFC membranes for comparison purposes. For IP, the PAN support was first impregnated with a diamine aqueous solution and then exposed to a TMC solution in *n*-hexane to produce the cross-linked PA layers. Process parameters such as monomer concentrations, reaction time, and drying conditions were optimized to show the best sodium chloride (NaCl) rejection of the resultant TFC membrane for P(*m*PDTA). Then, the same process parameters were applied to the fabrication of other PAs. In addition, the IP-assembled TFC membranes were prepared either on the pristine PAN or on HPAN to evaluate the effects of the support type on membrane performance.

The surface structures of the IP- and mLbL-assembled PA selective layers for the four PA systems are shown in Figure 3. The scanning electron microscope (SEM) images presented in Figure 3a illustrate the vast difference in the surface morphologies of the IP-assembled PAs using the same triacid chloride but slightly different structures of diamine, which is in good agreement with the observation by other researchers.[15] Keeping the other process variables

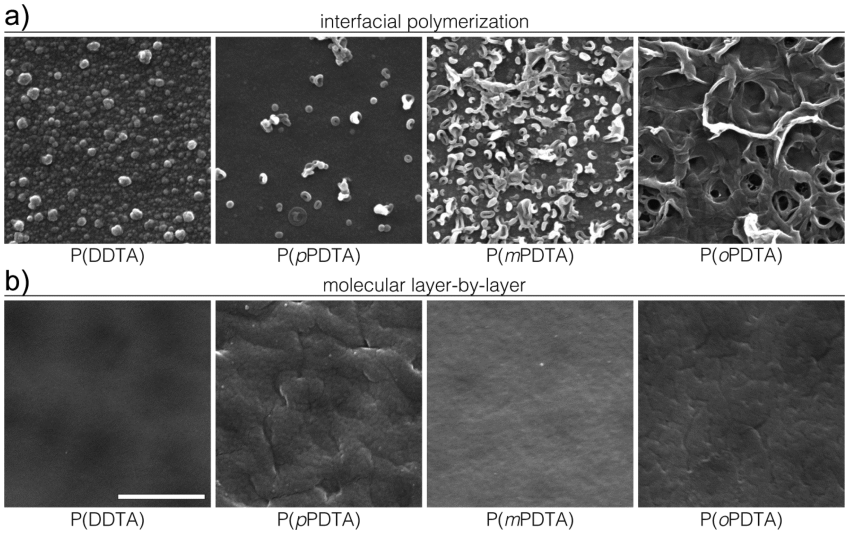

Figure 3. (a) SEM micrographs of the PA-selective layer surfaces fabricated *via* IP. (b) SEM micrographs of the PA selective layer surfaces fabricated *via* mLbL with the deposition cycle number of 15. The scale bar for all the micrographs is 1 μm.

fixed, even a small change in the amine monomer structure results in a dramatic variation in the surface morphology. This stems from the difference in the reactivity, solubility, and diffusivity depending on the monomer structure that significantly alters the IP mechanism,[10,16,17] which has profound impacts on the membrane performance including water flux, salt rejection, and fouling.[18] In contrast, the surfaces of the four mLbL-assembled PAs with chemistries identical to the ones made by IP are significantly smoother because mLbL is much less dependent on the reactivity, solubility, and diffusivity of the monomer species (Figure 3b).

Table 1 summarizes the XPS atomic contents of the PA selective layers prepared by IP and mLbL. Chemical compositions represented by the O/N ratio are nearly identical regardless of PA chemistry for the mLbL-assembled PAs. However, the O/N ratios for the IP-assembled PAs vary quite significantly depending on the PA chemistry.[19] Combined with the morphological analysis, these results demonstrate the uniqueness of mLbL, which is the ability to consistently fabricate PAs with polymer network structure and surface roughness that are independent of the specific PA chemistry.

To compare the TFC membrane performance between the two assembly approaches, we evaluated their performance *via* crossflow filtration using a NaCl (2000 ppm) aqueous solution. Figure 4 is a summary of the water flux (J_w) and NaCl rejection (R_s) of the mLbL-assembled TFC membranes as a function of the mLbL cycle number (x). The results show that membrane performance is controlled by the mLbL cycle number for the fully aromatic P(*p*PDTA), P(*m*PDTA), and P(*o*PDTA) systems. Using P(*m*PDTA) as an example, increasing the mLbL cycle number leads to a progressive decrease in the water flux and a progressive

TABLE 1. Atomic Compositions of the IP- and mLbL-Assembled PA selective Layers As Measured by XPS[a]

process	PA	C (%)	O (%)	N (%)	O/N ratio
IP	P(DDTA)	71.0	17.1	11.9	1.43
	P(*p*PDTA)	73.9	14.4	11.7	1.23
	P(*m*PDTA)	74.0	14.0	12.0	1.16
	P(*o*PDTA)	75.2	11.5	13.3	0.86
mLbL	P(DDTA)	71.5	15.5	13.0	1.20
	P(*p*PDTA)	75.6	13.5	10.9	1.24
	P(*m*PDTA)	74.7	13.9	11.4	1.22
	P(*o*PDTA)	73.7	14.2	12.1	1.17

[a] Each of the mLbL-assembled PA selective layers is made with 15 deposition cycles.

increase in the NaCl rejection. Both of these trends with the mLbL cycle number are consistent with our previous work on the mLbL-assembled P(*m*PDTA) TFC membranes.[14]

The observed performance trends with the mLbL cycle number can be quantitatively explained with a modified form of mass transport equations used to describe TFC membranes used in RO applications. For an applied pressure (Δp) exceeding the osmotic pressure ($\Delta\pi$) of the NaCl solution, the water flux of the polyelectrolyte LbL interlayer ($J_{w,0}$) and mLbL ($J_{w,x}$) TFC membranes can be described by a simplified resistance-in-series water permeation model[14,20]

$$J_{w,0} \approx \frac{\Delta p - \Delta\pi}{A_0^{-1}} \quad (1a)$$

$$J_{w,x} \approx \frac{\Delta p - \Delta\pi}{A_x^{-1} + A_0^{-1}} \quad (1b)$$

where the subscript x denotes the mLbL cycle number. The apparent water permeability coefficients of the LbL (A_0) and mLbL (A_x) TFC membranes are

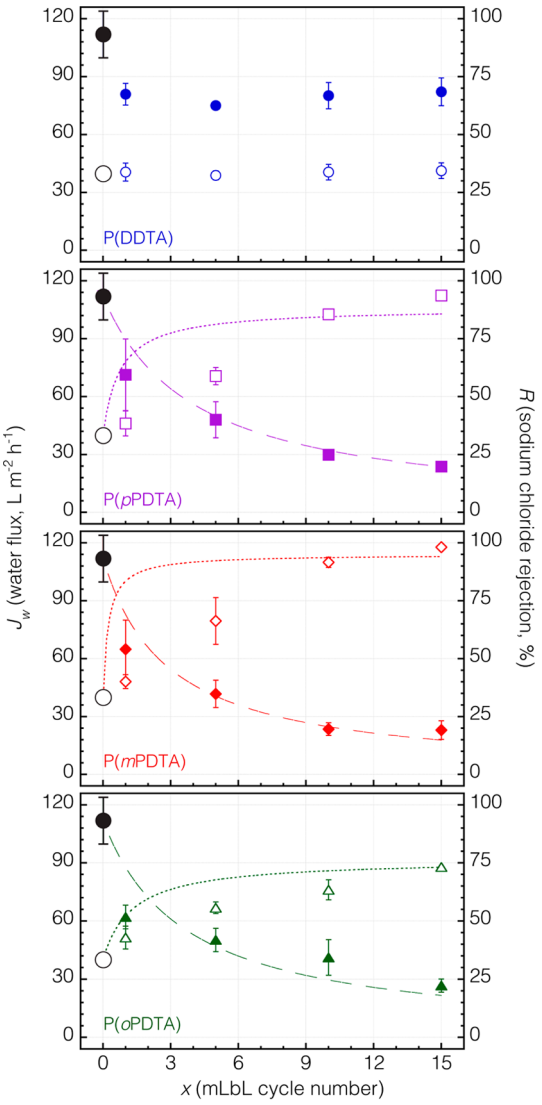

Figure 4. Water flux and NaCl rejection of the mLbL-assembled PA TFC membranes as a function of the mLbL cycle number. The closed symbols correspond to the water flux and the open symbols correspond to the salt rejection. The larger circles are the TFCs without the mLbL PA layer. The curves are fits to the water flux and NaCl rejection data using eq 3 and eq 6, respectively.

related to the layer thicknesses (h_0, h_x) and water permeabilities ($P_{w,0}$, $P_{w,x}$)[21]

$$A_0 = \frac{\nu_w}{RT}\frac{P_{w,0}}{h_0} \quad (2a)$$

$$A_x = \frac{\nu_w}{RT}\frac{P_{w,x}}{h_x} \quad (2b)$$

where ν_w is the molar volume of water, R is the gas constant, and T is the temperature. Substituting eqs 1a, 2a, and 2b into eq 1b yields the following expression for $J_{w,x}$:

$$J_{w,x} = J_{w,0}\left(1 + \frac{P_{w,0}h_x}{P_{w,x}h_0}\right)^{-1} \quad (3)$$

The resistance-in-series model also describes the NaCl rejection because it is a function of the water flux.[22] The NaCl rejection values of the LbL ($R_{s,0}$) and mLbL ($R_{s,x}$) TFC membranes are defined as

$$R_{s,0} = \frac{100\%}{1 + B_0 J_{w,0}^{-1}} \quad (4a)$$

$$R_{s,x} = \frac{100\%}{1 + \frac{J_{w,x}^{-1}}{B_0^{-1} + B_x^{-1}}} \quad (4b)$$

The apparent NaCl permeability coefficients of the LbL (B_0) and mLbL (B_x) TFC membranes are related to the layer thicknesses and NaCl permeabilities ($P_{s,0}$, $P_{s,x}$)[21]

$$B_0 = \frac{P_{s,0}}{h_0} \quad (5a)$$

$$B_x = \frac{P_{s,x}}{h_x} \quad (5b)$$

Substituting eqs 3, 4a, 5a, and 5b into eq 4b yields the following expression for $R_{s,x}$.

$$R_{s,x} = R_{s,0}\left(1 + \frac{J_{w,0}h_0}{P_{s,0}}\right)\left(\frac{1 + P_{w,0}h_x/P_{w,x}h_0}{1 + P_{s,o}h_x/P_{s,x}h_0} + \frac{J_{w,0}h_0}{P_{s,0}}\right)^{-1} \quad (6)$$

We use eqs 3 and 6 to describe the changes in the water flux and NaCl rejection of the mLbL-assembled TFC membranes with the mLbL cycle number. To fit these expressions with the results presented in Figure 4, we reduced the number of fitting parameters by assuming that $J_{w,0}$, $R_{s,0}$, $P_{w,0}$, $P_{w,x}$, $P_{s,0}$, $P_{s,x}$, and h_0 are constants and are independent of the mLbL cycle number (see the Supporting Information, S1). Thus, the mLbL layer thickness is the only variable that scales with the cycle number because it increases at a constant rate ($h_x = rx$, where r is thickness increment per mLbL cycle).[14] Except for the semiaromatic P(DDTA) that did not follow the solution-diffusion model, the close agreement between the fits with the experimental water flux data for the fully aromatic P(*p*PDTA), P(*m*PDTA), and P(*o*PDTA) suggests that our assumptions of the fitting parameters for describing water permeation are reasonable. The poor fits of the salt rejection data for the fully aromatic P(*p*PDTA), P(*m*PDTA), and P(*o*PDTA) at short mLbL cycle numbers suggest that $P_{s,x}$ cannot be treated as a constant. The cause of this cycle number dependent salt permeability at short cycle numbers will be discussed later on. These results show that mLbL can independently control the intrinsic properties *via* changing the polymer network chemistry and the extrinsic properties *via* changing the selective layer thickness while minimizing roughness, which is not achievable by conventional IP.

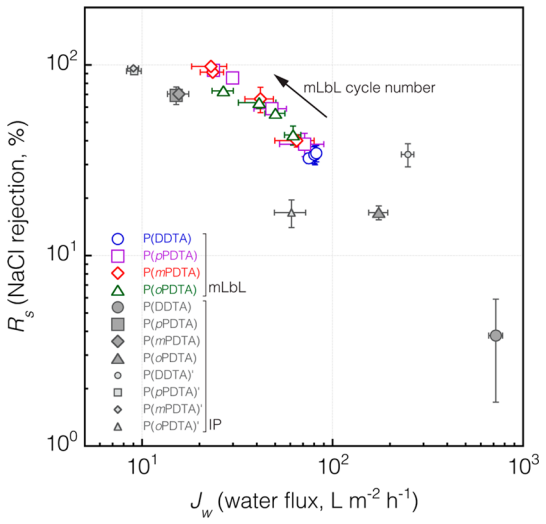

Figure 5. Plot of NaCl rejection *versus* water flux for all the TFC membranes investigated. Closed symbols correspond to the mLbL-assembled PA TFCs. The arrow indicates the change in the performance of the mLbL-assembled PAs with increasing mLbL cycle number. Filled symbols correspond to the IP-assembled PA TFCs prepared on PAN (smaller symbols) and HPAN (larger symbols) supports.

The exceptional water flux behavior of P(DDTA) with respect to the mLbL cycle number can be explained by the diamine monomer structure (piperazine, PIP) because the reactivity of this monomer affects its network structure and hence the layer growth rate. Compared with the other stiff aromatic diamine monomers, the higher chain flexibility of aliphatic PIP increases the propensity to form macrocycles that hinder the subsequent cross-linking reaction between PIP and TMC, making the mLbL film growth unfavorable.[23] This hypothesis is consistent with the membrane performance results where the water flux and NaCl rejection remain essentially unchanged beyond $x = 1$. In addition, the unfavorable mLbL film formation of P(DDTA) was further confirmed by no discernible difference in the selective layer thickness between the P(DDTA) membranes prepared with different mLbL cycle numbers (see the Supporting Information, S2).

Figure 5 is a summary of the NaCl rejection *versus* water flux for all the TFC membranes investigated. The results show an inverse relationship between the NaCl rejection and water flux. This trend is commonly observed in water desalination membranes and is often referred to as "performance trade-off", where an increase in the water flux results in a decrease in salt rejection.[21,24] Evaluating only the IP-assembled TFC membranes, the results show that the membrane performance strongly depends on the support type (pristine PAN/HPAN) as well as monomer chemistry.[8,10,11,25,26] The fully aromatic P(*p*PDTA) exhibited higher rejection than the semiaromatic P(DDTA) with the same isomeric position of the diamine, which is consistent with the previous report showing that higher aromaticity and thus increased chain stiffness imparts better selectivity.[27] Among the fully aromatic PAs, the P(*m*PDTA) exhibited the highest NaCl rejection, suggesting that the same isomeric positions (*meta*) of the reactive groups of diamine and the triacid chloride on aromatic rings result in a more selective PA structure.[15,27,28]

Regarding the effect of the support type, IP on a HPAN support typically resulted in lower salt rejection while exhibiting higher water flux than that on a PAN support. This result agrees with previous studies that showed IP on a more hydrophilic support often produces a TFC membrane with higher flux but lower rejection due to the difficulty in creating a defect-free PA selective layer.[10,11] We found that the IP-assembled P(DDTA) on a HPAN has the lowest NaCl rejection (R = 3.8 ± 2.1%) and the highest water flux (J_w = 720.5 ± 59.4 L m^{-2} h^{-1}), whereas the IP-assembled P(*m*PDTA) on a PAN has the one of the highest NaCl rejection rates (R = 96.0 ± 0.7%) but the lowest water flux (J_w = 9.0 ± 0.6 L m^{-2} h^{-1}). The performances of the other IP-assembled TFC membranes span between these two limits, which clearly illustrates that the IP-assembled TFC membranes have widely varying performance without any systematic trends with either the PA chemistry or support structure. These results are consistent with other IP-assembled TFC membranes where there is very little control over membrane performance because of the difficulty in controlling the various PA properties separately.

With the exception of semiaromatic P(DDTA), the mLbL-assembled TFC membranes clearly show a systematic change in the performance by simply varying the mLbL cycle number for each PA system. The results for the fully aromatic P(*p*PDTA), P(*m*PDTA), and P(*o*PDTA) show consistent "performance trade-offs" with the mLbL cycle number. The increase in NaCl rejection results in a progressive decrease in water flux (Figure 4), which is primarily attributed to the increase in the thickness and cross-linking density of the PA layer with increasing the mLbL cycle number. The key distinction between these PAs is the maximum attainable NaCl rejection, which is ultimately linked to the materials properties of the specific PA.[15−17,27,29] The full aromaticity and *meta*-positioning of the functional groups of P(*m*PDTA) results in the highest NaCl rejection among the mLbL-assembled PAs, similar to the results for the IP-assembled PAs. Importantly, all the fully aromatic mLbL-assembled PAs show higher NaCl rejection values than the IP-assembled PAs, which strongly suggests that mLbL facilitates the formation of PA selective layers with higher average cross-link densities. Not only does the mLbL-assembled P(*m*PDTA) have a higher NaCl rejection (R_s = 98.2 ± 0.6%), the water flux (J_w = 23.0 ± 4.8 L m^{-2} h^{-1}) is over 2.5 times greater than the IP-assembled P(*m*PDTA) (R_s = 96.0 ± 0.7%, J_w = 9.0 ± 0.6 L m^{-2} h^{-1}). This improvement is significant as it equates to a 2.5 times

increase in energy reduction because of the direct relationship between the water flux and applied pressure. Another interesting result is that the maximum attainable NaCl rejection of the mLbL-assembled P(*o*PDTA) is 73.2 ± 0.2%, which is over 4 times higher than that of the IP-assembled counterpart (16.8 ± 2.8%) and further highlights the advantageous attributes of mLbL. The superior separation performance of the mLbL-assembled membrane is attributed to thinner and more densely cross-linked structure of the PA selective layer realized *via* mLbL.[14] Compared with a commercial RO membrane (SWC4+, Nitto Denko), the mLbL-assembled P(*m*PDTA) membrane achieved slightly lower rejection than SWC4+ (R_s = 98.7 ± 0.9%) but comparable to or slightly higher water flux than SWC4+ (J_w = 21.3 ± 1.5 L m^{-2} h^{-1}). However, the salt rejection of the mLbL-assembled membrane is expected to be further improved by optimizing fabrication parameters, using additional additives and applying additional treaments similarly to commercial membranes.

The mLbL-assembled P(*m*PDTA) shows the upper limit of NaCl rejection and the lower limit of water flux (the highest NaCl rejection and lowest water flux) in the performance trade-off plot, although the upper NaCl rejection limit could be further enhanced by increasing the mLbL cycle number. The lower limit of NaCl rejection and upper limit of water flux of the mLbL-assembled membranes are determined by the substrate (the interlayer-coated support) structure as well as PA chemistry. Hence, the lower rejection (upper flux) limit is expected to be expanded by altering the interlayer and support structures and PA chemistry.

While Figure 5 is useful for evaluating the performance between the various membranes, it is difficult to understand the role of PA chemistry and structure on membrane transport because water flux and NaCl rejection are the industry-defined descriptors of membrane performance that depend on the particular measurement conditions. Instead, material properties including water permeability, salt permeability, and permselectivity are more appropriate descriptors of membrane transport because these properties are intrinsic to the particular PA.[10]

The water permeability of dense TFC membranes is related to the water flux as defined by eqs 1 and 2.

$$P_w = \frac{J_w}{(\Delta p - \Delta\pi)} \frac{RTh}{\nu_w} \quad (7)$$

The salt permeability of dense water desalination membranes is related to the salt flux ($J_s = P_s \Delta C_s / h$), which can be calculated from the measured values of water flux and NaCl rejection ($J_s = J_w \Delta c_s((100\%/R_s) - 1)$).

$$P_s = J_w h \left(\frac{100\%}{R_s} - 1 \right) \quad (8)$$

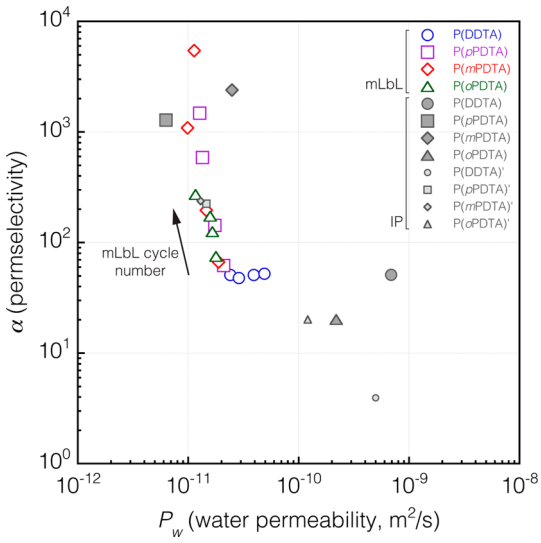

Figure 6. Plot of permselectivity *versus* water permeability, which is commonly referred to as a "performance trade-off" plot, for all TFC membranes investigated. The arrow indicates the change in the performance with increasing mLbL cycle number. Filled symbols correspond to the IP-assembled PA TFCs prepared on PAN (smaller symbols) and HPAN (larger symbols) supports.

Permselectivity (α) is a dimensionless quantity that is defined as the ratio of the water permeability to the salt permeability.[21]

$$\alpha = \frac{P_w}{P_s} \quad (9)$$

Calculating these intrinsic properties requires information about the PA layer thickness. Determining the thickness of the mLbL-assembled PAs is straightforward since these materials have minimal surface roughness,[13,14,30,31] and the thickness of these layers was calculated on the basis of our previous works on the growth rate of the particular PA as a function of the mLbL cycle number (see the Supporting Information, S3).[14,30,31] In contrast, there is a significant degree of uncertainty in determining the thickness of the IP-assembled PAs due to their high surface roughness. As a first order approximation, the thickness of the IP-assembled PAs was determined by analyzing the average sample cross-section *via* transmission electron microscopy (see the Supporting Information, S3 and S4). The water permeabilities, salt permeabilities, and permselectivities for all the TFC membranes are then calculated using eqs 7, 8, and 9, respectively.

We evaluate the intrinsic transport properties of the TFC membranes in the form of a "performance trade-off" plot by comparing the permselectivity *versus* the water permeability (Figure 6). The results illustrate the vast and random variation in the transport properties of the IP-assembled TFC membranes with PA chemistry and support type. Importantly, the fully aromatic IP-assembled PAs exhibited inferior permselectivity to the mLbL-assembled counterparts.

The "performance trade-off" plot sheds several insights of the mLbL-assembled TFC membranes. First, the performance trade-off trend is also observed for all three fully aromatic PAs. We see that an increase in permselectivity leads to a decrease in water permeability and *vice versa*. This observation is consistent with the performance trade-off trend observed for other membranes.[21] The interesting result is that performance trade-off trend with the mLbL cycle number is very steep. In other words, the decrease in the salt permeability with the cycle number being significantly greater than that of the water permeability for a particular fully aromatic PA. Since the water and salt permeabilities are intrinsic properties that are directly related to the diffusion and solubility coefficients for a particular PA network chemistry, these results imply that the fully aromatic PA network structure can be controlled indirectly *via* the mLbL cycle number. We speculate that the polymer network structure is incomplete at short mLbL cycle numbers and becomes fully cross-linked at higher cycle numbers. The fact that the water permeability does not change significantly with the mLbL cycle number suggests that the water permeability (the product of water diffusion coefficient and solubility) is less dependent on the cross-link density compared with the salt permeability. This assumption of approximately invariant water permeability with the mLbL cycle number is supported by the good agreement between the water flux results (Figure 4) and the data fits using eq 3 where we have assumed a constant water permeability coefficient for a particular PA. This assumption is not true in the case of the salt permeability. Here we find that the salt permeability decreases quite significantly and spans up to 2 orders in magnitude depending on the particular PA. The poor fits of the salt rejection results (Figure 4) using eq 6 confirm the strong dependence of salt permeability with the mLbL cycle number and suggests that cross-linking density of the PA have large impacts to the separation of salt ions. This control of the intrinsic properties has not been explored previously for a particular PA because of the inherent limitation of IP in controlling the network structure of the PA. While we will study the effects of the mLbL cycle number on the cross-linking density of the PA network in detail in the future, the current results indicate that the cross-linking density increases with the mLbL cycle number, which leads to the observed performance trade-off trends. Based on performance trade-off results from commercial TFC membranes,[21] we speculate that the permselectivity could increase by another order of magnitude ($\sim 10^5$ to 10^6) by further increasing cross-linking density (increasing the mLbL cycle number) until it reaches a constant value.

Second, the permselectivity of P(*m*PDTA) is intrinsically superior when compared to the other three mLbL-assembled PAs, further confirming that the aromatic monomer pairs with the same isomeric position (*meta*-positioned) of the functional groups result in the optimum molecular structure that exhibits the best permselectivity.[15,27,28] We suggest that cross-linking of the same *meta*-positioned functional groups facilitates the formation of a PA network structure that best optimizes performance trade-off between water flux and permselectivity. This argument is supported by a previous study on the swelling of the mLbL-assembled PA thin films showing that the water swelling ratio for P(*m*PDTA) is intermediate to the more swollen P(*p*PDTA) and the less swollen P(*o*PDTA).[31] According to the solution-diffusion model, a membrane that swells more is expected to have higher water permeability because it is directly related to the water solubility. Combined with the performance trade-off argument of higher water permeability resulting in lower permselectivity, these results would indicate that P(*m*PDTA) has permselectivity that is superior to P(*p*PDTA) and water permeability that is superior to P(*o*PDTA). All these results reinforce the notion that P(*m*PDTA)-based TFC membranes are the state-of-the-art selective layers for seawater desalination.[2,3]

Third, the solution-diffusion model does not appear to be the appropriate model in describing the performance of P(DDTA). The permselectivity results from the performance trade-off plot (Figure 5), along with NaCl rejection *versus* the water flux data (Figure 4), suggest that the performance of P(DDTA) does not scale with the mLbL cycle number. The aforementioned inefficient mLbL film growth for P(DDTA) could account for the deviation from prediction according to the solution-diffusion model. Our result is not too surprising given the literature precedence suggesting that the transport mechanism of NF-grade P(DDTA)-based TFC membranes involves both solution-diffusion and pore flow models.[32]

Fourth, the mLbL approach enables more accurate evaluation of performance trade-off for water desalination membranes. The IP-assembled membranes have significantly higher surface roughness than the mLbL analogues. The high surface roughness of the IP-assembled membranes originates from the uncontrolled reaction at multiple interfaces by the monomer diffusion-controlled mechanism,[6] while the smooth surface of the mLbL-assembled membranes is attributed to the controlled reaction at a single interface by the stoichiometry-limiting mechanism.[14,23] This morphological feature (roughness) can affect permeation in two ways. An increase in surface area for water permeation will increase the total water flux, which is the reason for commercial membranes to adopt the spiral wound membrane module design *versus* flat-sheet membrane design. Our calculations (see Supporting Information, S5) show that a rough membrane whose surface is densely packed with high-aspect ratio roughness features can increase

the surface area by 10−100 times that of a smooth membrane. Another effect of surface roughness is that the local properties such as thickness and permeability coefficients of the membrane may be different than smooth regions of the membrane, which would raise the question whether the entire membrane has the same transport properties. These uncertainties for rough membranes will affect the calculated water and salt permeability coefficients required to construct the performance trade-off plot, which also limits the development of structure−property relationships for these materials.

CONCLUSION

We have demonstrated that mLbL enables fabrication of various PA-based water desalination membranes with well-defined and deconvoluted intrinsic and extrinsic properties. Our results verify that controlling the selective layer thickness, roughness, and chemical composition is critical for water desalination performance. The mLbL approach provides a rational and tailor-made approach to designing water desalination membranes that can satisfy the performance requirements for a particular application. From a fundamental perspective, mLbL enables fabrication of model materials that allow one to gain insights into the transport mechanism as well as the key polymer properties that control transport in water desalination membranes. For example, mLbL enables deconvolution of the effect of charge density and cross-link density because we can systematically vary these properties by incorporation of monomers with different degrees of functionality (difunctional *versus* trifunctional) and chemistry. One other subtle but important attribute of mLbL is that it is an all organic solvent synthesis, which implies that mLbL is not limited to the current set of triacid chloride and diamine monomer chemistries. Scalability remains the primary drawback for mLbL since the slow growth rate of the selective layer is not practical for commercial implementation. Work is currently underway to explore the use of multifunctional monomers that can significantly expedite the growth rate of the selective layer while maintaining the key attributes of mLbL. The membrane stability is another critical issue to be resolved since the structural deformation and delamination of the polyelectrolyte bilayer used as an interlayer could occur at high ionic strengths (*i.e.*, NaCl > 10000 ppm) or extreme pH conditions (*i.e.*, pH < 3 or pH > 10). We are evaluating the membrane stabilty at various solution chemistries (ionic strengths and pHs) along with exploring the strategy to improve the membrane stability.

METHODS

General Methods. Certain commercial equipment, instruments, or materials are identified in this paper in order to specify the experimental procedure adequately. Such identification is not intended to imply recommendation or endorsement by the National Institute of Standards and Technology, nor is it intended to imply that the materials or equipment identified are necessarily the best available for the purpose. The error bars represent one standard deviation of the data, which is taken as the uncertainty of the measurement.

Materials. The following chemicals were used as received: branched polyethylenimine (PEI, M_w = 750,000 g mol^{-1}, Sigma-Aldrich), poly(acrylic acid) (PAA, M_w = 100,000 g mol^{-1}, Sigma-Aldrich), diethylenediamine (commonly called piperazine, PIP, Sigma-Aldrich), *p*-phenylenediamine (PPD, Sigma-Aldrich), *m*-phenylenediamine (MPD, Sigma-Aldrich), *o*-phenylenediamine (OPD, Sigma-Aldrich), trimesoyl chloride (TMC, Sigma-Aldrich), sodium chloride (NaCl, Junsei Chemical Co.), sodium hydroxide (NaOH, Daejung Chemical Co.), toluene (>95%, J.T. Baker), *n*-hexane (>95%, J.T. Baker), and acetone (>95%, J.T. Baker). Deionized (DI) water (18.2 Ω) was prepared in a Millipore Milli-Q purification system. Polyacrylonitrile (PAN) ultrafiltration membranes (PAN 50) and a seawater RO membrane (SWC4+) were obtained from Sepro Membranes, Inc., and Nitto Denko, respectively.

Membrane Preparation. A series of TFC membranes were prepared *via* the mLbL approach using TMC and different diamines (PIP, OPD, MPD, and PPD). First, a PAN support was hydrolyzed in a NaOH (2.0 M) aqueous solution at 50 °C for 2 h to increase the surface negative charge and hydrophilicity. Then, a single bilayer of polyelectrolyte layer-by-layer assembly (LbL) was prepared on the hydrolyzed PAN (HPAN) as an interlayer. The negatively charged HPAN was first soaked into a cationic PEI (0.1 wt %) aqueous solution containing NaCl (0.5 M, pH = 10.6) for 15 min and then rinsed twice with DI water. Subsequently, the PEI-coated HPAN was dipped into an anionic PAA (0.1 wt %) aqueous solution containing NaCl (0.5 M, pH = 3.5) for 10 min, followed by rinsing twice with DI water. Next, the PA selective layer was created on the PEI/PAA-coated PAN support by alternatively depositing diamine and TMC monomers. The membrane support was soaked in the diamine monomer (1.0 wt %) solution in toluene for 30 s and subsequently rinsed with acetone to remove the unreacted amine. PIP, MPD, and OPD monomer solutions were prepared by dissolving the diamine monomer in toluene, while PPD was dissolved in a mixture of toluene and acetone (80/20 wt %) owing to its limited solubility in toluene. Then, the membranes were dipped into a TMC (1.0 wt %) solution in toluene for 30 s, followed by rinsing with toluene to complete one mLbL deposition cycle. This process was repeated to obtain the desired number of deposition cycles. After completion of the mLbL deposition, the prepared membranes were dried at 70 °C for 2 min and stored in DI water prior to test. TFC membranes were also prepared on pristine PAN and HPAN supports by conventional interfacial polymerization (IP) as controls. A diamine (2.0 wt %) aqueous solution was poured onto a PAN support and then drained off after 3 min. The excess amine solution was removed with an air knife. Then, a TMC (0.05 wt %) solution in *n*-hexane was poured onto the membrane and allowed to react for 1 min. The polymerization reaction was terminated by rinsing the membrane with pure *n*-hexane. The prepared membranes were dried at 70 °C for 2 min and stored in DI water prior to test.

Membrane Characterization. X-ray photoelectron spectroscopy (XPS) was used to characterize the chemical structures of the mLbL- and IP-assembled PA selective layers. XPS spectra were collected on a PHI-5000 Versaprobe spectrometer using monochromatic Al K_α radiation at 1.49 keV. The surface morphologies of the PA layers were examined using scanning electron microscopy (SEM, FEI Inspect F50), and SEM micrographs were obtained at an accelerating voltage of 10 kV. Cross-sectional images of TFC membranes were obtained using transmission electron microscopy (TEM, FEI Titan TM 80−300).

To prepare TEM samples, the TFC membranes were embedded in Epon resin (EMbed 812) and then cured at 60 °C for 24 h. Ultrathin membrane slices were cut on an ultramicrotome (Reichert Ultracut S) and mounted onto copper grids. The cross sections were imaged at an accelerating voltage of 300 kV.

Membrane Performance. Membrane performance (water flux and salt rejection) was measured by permeating a NaCl solution (2,000 ppm) at pH 5.8 in a cross-flow filtration apparatus with an effective permeation area (A = 14.5 cm^2). All performance measurements were carried out at an operating pressure of 15.5 bar, a flow rate of 1 L min^{-1}, and an operating temperature of 25 °C. Performance data were collected after the system had reached steady-state conditions. Water flux (J_w, L m^{-2} h^{-1}) was calculated from the amount of the collected permeate (V) for a fixed period of time (t) as given by $J_w = V/At$. NaCl rejection (R_s, %) was determined from the salt concentrations of the feed (C_f) and permeate (C_p) solutions, which were measured with a conductivity meter (Ultrameter II, Myron L. Co.) using the equation $R_s = 100\% \times (1 - C_p/C_f)$.

Conflict of Interest: The authors declare no competing financial interest.

Supporting Information Available: Cross-sectional TEM micrographs of the selective layers of TFC membranes. This material is available free of charge *via* the Internet at http://pubs.acs.org.

Acknowledgment. This work was supported by the National Research Foundation of Korea grant funded by the Korea government (MSIP) (No. 2014R1A1A1003197). J.S.L. acknowledges financial support from the Korea CCS R&D Center (KCRC) (No. 2014M1A8A1049315), Republic of Korea. Official contribution of the National Institute of Standards and Technology.

REFERENCES AND NOTES

1. Shannon, M. A.; Bohn, P. W.; Elimelech, M.; Georgiadis, J. G.; Marinas, B. J.; Mayes, A. M. Science and Technology for Water Purification in the Coming Decades. *Nature* **2008**, *452*, 301–310.
2. Elimelech, M.; Phillip, W. A. The Future of Seawater Desalination: Energy, Technology, and the Environment. *Science* **2011**, *333*, 712–717.
3. Geise, G. M.; Lee, H. S.; Miller, D. J.; Freeman, B. D.; Mcgrath, J. E.; Paul, D. R. Water Purification by Membranes: The Role of Polymer Science. *J. Polym. Sci., Part B: Polym. Phys.* **2010**, *48*, 1685–1718.
4. Cadotte, J. E.; King, R. S.; Majerle, R. J.; Petersen, R. J. Interfacial Synthesis in the Preparation of Reverse-Osmosis Membranes. *J. Macromol. Sci. Part - Chem.* **1981**, *A15*, 727–755.
5. Chai, G. Y.; Krantz, W. B. Formation and Characterization of Polyamide Membranes *via* Interfacial Polymerization. *J. Membr. Sci.* **1994**, *93*, 175–192.
6. Freger, V. Nanoscale Heterogeneity of Polyamide Membranes Formed by Interfacial Polymerization. *Langmuir* **2003**, *19*, 4791–4797.
7. Xie, W.; Geise, G. M.; Freeman, B. D.; Lee, H. S.; Byun, G.; McGrath, J. E. Polyamide Interfacial Composite Membranes Prepared from m-phenylene Diamine, Trimesoyl Chloride and a New Disulfonated Diamine. *J. Membr. Sci.* **2012**, *403*, 152–161.
8. Huang, L. W.; Bui, N. N.; Meyering, M. T.; Hamlin, T. J.; McCutcheon, J. R. Novel Hydrophilic Nylon 6,6 Microfiltration Membrane Supported Thin Film Composite Membranes for Engineered Osmosis. *J. Membr. Sci.* **2013**, *437*, 141–149.
9. Kwak, S. Y.; Jung, S. G.; Kim, S. H. Structure−Motion−Performance Relationship of Flux-Enhanced Reverse Osmosis (RO) Membranes Composed of Aromatic Polyamide Thin Films. *Environ. Sci. Technol.* **2001**, *35*, 4334–4340.
10. Ghosh, A. K.; Jeong, B. H.; Huang, X. F.; Hoek, E. M. V. Impacts of Reaction and Curing Conditions on Polyamide Composite Reverse Osmosis Membrane Properties. *J. Membr. Sci.* **2008**, *311*, 34–45.
11. Klaysom, C.; Hermans, S.; Gahlaut, A.; Van Craenenbroeck, S.; Vankelecom, I. F. J. Polyamide/Polyacrylonitrile (PA/PAN) Thin Film Composite Osmosis Membranes: Film Optimization, Characterization and Performance Evaluation. *J. Membr. Sci.* **2013**, *445*, 25–33.
12. Wang, T. Y.; Dai, L.; Zhang, Q. F.; Li, A.; Zhang, S. B. Effects of Acyl Chloride Monomer Functionality on the Properties of Polyamide Reverse Osmosis (RO) Membrane. *J. Membr. Sci.* **2013**, *440*, 48–57.
13. Johnson, P. M.; Yoon, J.; Kelly, J. Y.; Howarter, J. A.; Stafford, C. M. Molecular Layer-by-Layer Deposition of Highly Cross-linked Polyamide Films. *J. Polym. Sci., Part B: Polym. Phys.* **2012**, *50*, 168–173.
14. Gu, J. E.; Lee, S.; Stafford, C. M.; Lee, J. S.; Choi, W.; Kim, B. Y.; Baek, K. Y.; Chan, E. P.; Chung, J. Y.; Bang, J.; *et al.* Molecular Layer-by-Layer Assembled Thin-Film Composite Membranes for Water Desalination. *Adv. Mater.* **2013**, *25*, 4778–4782.
15. Kwak, S. Y.; Jung, S. G.; Yoon, Y. S.; Ihm, D. W. Details of Surface Features in Aromatic Polyamide Reverse Osmosis Membranes Characterized by Scanning Electron and Atomic Force Microscopy. *J. Polym. Sci., Part B: Polym. Phys.* **1999**, *37*, 1429–1440.
16. Li, L.; Zhang, S. B.; Zhang, X. S.; Zheng, G. D. Polyamide Thin Film Composite Membranes Prepared from Isomeric Biphenyl Tetraacyl Chloride and m-phenylenediamine. *J. Membr. Sci.* **2008**, *315*, 20–27.
17. Roh, I. J. Effect of the Physicochemical Properties on the Permeation Performance in Fully Aromatic Crosslinked Polyamide Thin Films. *J. Appl. Polym. Sci.* **2003**, *87*, 569–576.
18. Verissimo, S.; Peinemann, K. V.; Bordado, J. Influence of the Diamine Structure on the Nanofiltration Performance, Surface Morphology and Surface Charge of the Composite Polyamide Membranes. *J. Membr. Sci.* **2006**, *279*, 266–275.
19. Tang, C. Y. Y.; Kwon, Y. N.; Leckie, J. O. Effect of Membrane Chemistry and Coating Layer on Physiochemical Properties of Thin Film Composite Polyamide RO and NF Membranes I. FTIR and XPS Characterization of Polyamide and Coating Layer Chemistry. *Desalination* **2009**, *242*, 149–167.
20. Chan, E. P.; Mulhearn, W. D.; Huang, Y. R.; Lee, J. H.; Lee, D.; Stafford, C. M. Tailoring the Permselectivity of Water Desalination Membranes *via* Nanoparticle Assembly. *Langmuir* **2014**, *30*, 611–616.
21. Geise, G. M.; Paul, D. R.; Freeman, B. D. Fundamental Water and Salt Transport Properties of Polymeric Materials. *Prog. Polym. Sci.* **2014**, *39*, 1–42.
22. Baker, R. W. *Membrane Technology and Application*; John Wiley & Sons: Chichester, 2004.
23. Lomadze, N.; Perez, M.; Prucker, O.; Ruhe, J.; Reinecke, H. Step-and-Repeat Assembly of Molecularly Controlled Ultrathin Polyaramide Layers. *Macromolecules* **2010**, *43*, 9056–9062.
24. Kong, C. L.; Kanezashi, M.; Yamomoto, T.; Shintani, T.; Tsuru, T. Controlled Synthesis of High Performance Polyamide Membrane with Thin Dense Layer for Water Desalination. *J. Membr. Sci.* **2010**, *362*, 76–80.
25. Jimenez-Solomon, M. F.; Gorgojo, P.; Munoz-Ibanez, M.; Livingston, A. G. Beneath the Surface: Influence of Supports on Thin Film Composite Membranes by Interfacial Polymerization for Organic Solvent Nanofiltration. *J. Membr. Sci.* **2013**, *448*, 102–113.
26. Singh, P. S.; Joshi, S. V.; Trivedi, J. J.; Devmurari, C. V.; Rao, A. P.; Ghosh, P. K. Probing the Structural Variations of Thin Film Composite RO Membranes Obtained by Coating Polyamide over Polysulfone Membranes of Different Pore Dimensions. *J. Membr. Sci.* **2006**, *278*, 19–25.
27. Kim, C. K.; Kim, J. H.; Roh, I. J.; Kim, J. J. The Changes of Membrane Performance with Polyamide Molecular Structure in the Reverse Osmosis Process. *J. Membr. Sci.* **2000**, *165*, 189–199.
28. Roh, I. J.; Park, S. Y.; Kim, J. J.; Kim, C. K. Effects of the Polyamide Molecular Structure on the Performance of Reverse Osmosis Membranes. *J. Polym. Sci., Part B: Polym. Phys.* **1998**, *36*, 1821–1830.

29. Liu, M. H.; Wu, D. H.; Yu, S. C.; Gao, C. J. Influence of the Polyacyl Chloride Structure on the Reverse Osmosis Performance, Surface Properties and Chlorine Stability of the Thin-Film Composite Polyamide Membranes. *J. Membr. Sci.* **2009**, *326*, 205–214.
30. Chan, E. P.; Lee, J. H.; Chung, J. Y.; Stafford, C. M. An Automated Spin-Assisted Approach for Molecular Layer-by-Layer Assembly of Crosslinked Polymer Thin Films. *Rev. Sci. Instrum.* **2012**, *83*, 114102.
31. Chan, E. P.; Young, A. P.; Lee, J. H.; Stafford, C. M. Swelling of Ultrathin Molecular Layer-by-Layer Polyamide Water Desalination Membranes. *J. Polym. Sci., Part B: Polym. Phys.* **2013**, *51*, 1647–1655.
32. Li, L.; Zhang, S. B.; Zhang, X. S. Preparation and Characterization of Poly(piperazineamide) Composite Nanofiltration Membrane by Interfacial Polymerization of 3,3′,5,5′-Biphenyl Tetraacyl Chloride and Piperazine. *J. Membr. Sci.* **2009**, *335*, 133–139.